Applied Surface Science 457 (2018) 644–654

Contents lists available at ScienceDirect

Applied Surface Science

journal homepage: www.elsevier.com/locate/apsusc

Full Length Article

Synthesis and characterization of TiO_2 films onto AISI 304 metallic meshes and their application in the decomposition of the endocrine-disrupting alkylphenolic chemicals

C. de M. da Trindade[a,b], S.W. da Silva[a], J.P. Bortolozzi[b], E.D. Banús[b], A.M. Bernardes[a,*], M.A. Ulla[b]

[a] Universidade Federal do Rio Grande do Sul – UFRGS – (PPGE3M, Lacor), Av. Bento Gonçalves, 9500 Porto Alegre, RS, Brazil
[b] Instituto de Investigaciones en Catálisis y Petroquímica – INCAPE (UNL – CONICET), Santiago del Estero 2829, 3000 Santa Fe, Argentina

ARTICLE INFO

Keywords:
Titanium dioxide
Metallic mesh
Organic and inorganic additives
Photocatalysis
Contaminants of emerging concern
Nonylphenol ethoxylate

ABSTRACT

This contribution describes the influence of the ratio of polyvinyl alcohol (PVA), TiO_2 and wire opening of metal meshes for the construction of a structured catalyst with a uniform coating, that present high adherence and photocatalytic activity. The best coating results were observed for a PVA/TiO_2 mass ratio of 0.37 and mesh opening of 546 μm. This coating exhibited a uniform distribution, high adherence and the maintenance of anatase and rutile phases. These aspects can be related to three variables: (i) the structure of the stainless-steel metal mesh, (ii) the thermal pretreatment and (iii) the amount of organic additive (PVA/TiO_2 ratio) employed in the suspensions. The most important achievement of this work was the fabrication of a structured catalyst with excellent stability, without losing activity for the degradation of endocrine-disrupting nonylphenol ethoxylate (NP_4EO) in synthetic solution, without poisoning of the catalytic surface. In fact, the results showed that even with a real wastewater matrix, a high photocatalytic activity for NP_4EO degradation (91%) was obtained, meaning that this structured catalyst can be applied to solve serious environmental problems as the contamination by endocrine-disrupting NP_4EO, without subsequent catalyst recovery and recycle steps.

1. Introduction

The nonylphenol ethoxylate (NP_nEO) is an important pollutant, since it is widely used in the composition of emulsifiers, detergents, surface modifiers as well as in flotation and dispersing agents in the industry [1]. Although these uses, when the ethoxylate number is equal or lower 4, the nonylphenol ethoxylate can act as an endocrine-disrupter [2,3] leading to toxicity [4,5].

Considering the treatment methods, NP_nEO revealed high resistance to the photolytic degradation process, as demonstrated by some studies conducted by Neamtu et al. [6] and Chen et al. [7]. One way to reduce the toxicity effect is the application of advanced oxidation processes (AOPs) that can lead to mineralization, as demonstrated by studies using gamma radiation/H_2O_2 treatment [8] and photoelectrocatalysis [9].

In this context, photocatalysis can be used for NP_nEO mineralization, either as a dispersed powder or as a film coating onto a substrate. Some studies were conducted to degrade nonylphenol ethoxylate-9 (NP_9EO) under UV and solar irradiation by ZnO particles (flower and pseudo sphere forms) [10]. However, the use of powder catalysts has the inconvenience of requiring, at the end of the treatment process, a recovery step. Besides, the particles and nanoparticles released in the environment can be highly toxic [10]. Therefore, the utilization as supported TiO_2 films has increased significance [11–13].

TiO_2 films supported onto metallic foams were previously studied by our group [14]. However, the TiO_2 film showed deep cracks and the TiO_2/foam structured catalyst presented poisoning after seven cycles, when it was used in a photocatalytic process. The poisoning was attributed to the presence of byproducts. They generated organic films deposited onto the TiO_2-foam surface during the photocatalytic process, reducing the active surface of the catalyst. In addition, geometric characteristics of the foams, their small pore sizes (diameter: 0.5 mm) and their assemblage in the photo-reactor were considered responsible for this problem [14].

The use of metallic meshes as structured substrates could solve this trouble, since they present surface area up to 100 $m^2\,m^{-3}$, which allows the use of a high amount of catalytic load in a small volume [15–17]. They also present easy manipulation of the mesh opening size, which

* Corresponding author at: Av. Bento Gonçalves, 9500 – Setor 4 – Prédio 43426 – Sala 109, Porto Alegre, Rio Grande do Sul, Brazil.
E-mail address: amb@ufrgs.br (A.M. Bernardes).

https://doi.org/10.1016/j.apsusc.2018.06.287
Received 5 April 2018; Received in revised form 4 June 2018; Accepted 29 June 2018
Available online 30 June 2018

allows controlling the resistance to flow, heat and mass transfer and to the temperature distribution [16,17].

The supported catalytic film can be obtained by physical or chemical synthesis methods. Washcoating is one of the most used method to obtain catalytic coatings on structured substrates, due to the easiness of preparation. However, when the substrate is a metallic material, the difference of thermal expansion coefficients between substrate and coating could be a serious problem, thus promoting low quality films [14,15,18]. There are some options to solve this adherence trouble, such as thermal passivation of the substrate, the addition of another solid or an organic additive in the synthesis film [19].

The addition of another solid is a way of improving the thermal stability [17]. Studies have reported that the addition of ZrO_2 nanoparticles promoted changes in the surface of the catalyst, which became smoother, more uniform, with smaller cracks than the ones obtained with pure TiO_2 films. Interspaces of TiO_2 particles and agglomerations may be reduced with the addition of ZrO_2 [20,21]. Besides that, an organic additive as polyvinyl alcohol (PVA) leads to an increase in the viscosity and the surface tension of the suspensions, due to the presence of hydroxyl groups in its structure [22]. In fact, hydrogen bonds may also exist between the PVA chains and the oxidized surface of the substrate, resulting in a polymeric fixation between TiO_2 catalyst and the metallic substrate [22–25].

In this context, the motivation of the present work was to evaluate the influence of different PVA/TiO_2 ratios and wire opening of metallic meshes, aiming to the production of an efficient structured catalyst with uniform TiO_2 coating with high adherence to the substrate. The structured catalyst with best morphological and physicochemical characteristics was employed in the photocatalytic degradation of NP_4EO in two different water matrices: synthetic solution and municipal wastewater after activated sludge treatment. The last experiment was carried out to evaluate the effect of a real water matrix on the activity of structured system.

2. Experimental

The experimental procedure is shown in supplementary content (Fig. S1).

Supplementary data associated with this article can be found, in the online version, at https://doi.org/10.1016/j.apsusc.2018.06.287.

2.1. Chemicals and reagents

Reagents with analytical grade were used for the catalyst preparation. Polyvinyl alcohol (PVA), colloidal suspension of zirconium oxide nanoparticles (ZrO_2, 20 wt%, dp = 100 nm) and TiO_2 P25 Degussa powder (AEROXIDE®, 50 $m^2 g^{-1}$, 80% anatase and 20% rutile, dp = 21 nm) were purchased from Sigma-Aldrich, Nyacol® and Evonik, respectively.

The preparation of solutions used in chromatography analysis was made with ultra-pure water with a resistivity 18.2 MΩ cm from milli-Q system (Millipore) and Na_2CO_3, $NaHCO_3$ and H_2SO_4 with analytical grade (Merck). The NP_4EO used in the photocatalytic experiments was purchased from Oxiteno.

2.2. Metallic mesh pretreatment

Two metallic meshes of AISI 304 stainless steel designated as M1 (mesh opening 546 μm) and M2 (mesh opening 1514 μm) were used as substrates. Their main characteristics are presented in the supplementary content (Table S1).

The metallic meshes were washed in an ultrasonic bath during 30 min in detergent-water and for 30 min in acetone to remove organic and inorganic impurities. After each cleaning step the metallic meshes were dried in an oven at 120 °C for 60 min. Then, they were calcined at 900 °C for 120 min (10 °C min^{-1}) in a muffle furnace and finally cooled down to room temperature. After this step an oxide layer on the metal substrate is produced, which contributes to enhance the adherence of the catalyst to the structure [14], since a surface roughness is generated [18].

2.3. Catalytic suspensions

In a simple synthesis process, a determined amount of PVA was dissolved at 70 °C in 121.2 g of deionized water under magnetic stirring, until its complete dissolution. The clear solution was cooled down to room temperature. Then, 40.8 g of colloidal suspension of ZrO_2 nanoparticles and 9.6 g of TiO_2 were added. After that, the suspension was stirred for 24 h before using. The mass of PVA was varied, resulting in a series of suspensions prepared with PVA/TiO_2 mass ratio of 0.19, 0.28 and 0.37, designated as TPa, TPb and TPc, respectively.

2.4. Catalyst immobilization onto the metallic mesh

A washcoating method was used to immobilize TiO_2 onto the surface of the metallic meshes. The immobilization of TiO_2 was carried out in four steps: (1) Immersion: the pretreated metallic meshes were placed vertically into the catalytic suspension under magnetic stirring and taken out after 1 min. (2) Blowing: the meshes were softly blown with air flow to remove the suspension excess. These two steps were carried out for both sides of the metallic mesh. (3) Drying: the samples were dried at 120 °C for 60 min. (4) Calcination: finally, they were calcined at 500 °C for 60 min with a heating rate of 1 °C min^{-1}. The complete cycle immersion – blowing – drying – calcination was repeated until the desired weight was achieved.

2.5. Characterization

The phases present in the surface of the pretreated metallic meshes and of the structured catalyst were analyzed by Laser Raman Spectroscopy (LRS). A Horiba-Jobin-Yvon instrument was employed to obtain the spectra. The excitation wavelength was 532.13 nm (Spectra Physics diode pump solid state laser, with power set at 30 mW). Several spectra were acquired for each sample to ensure reliable results.

The surface morphology of the pretreated metallic meshes and the structured catalyst surfaces, were analyzed by optical microscopy (OM) with a Leica S8 APO stereo-microscope equipped with a Leica LC3 digital camera and LAS EZ software. Scanning electron microscopy (SEM) and Energy-dispersive of X-ray Analysis (EDX) were performed with a Phenom world – PRO X equipment.

X-ray diffraction (XRD) was carried out on the structured catalyst with a Shimadzu XD-D1 diffractometer. Crystalline phases were identified using Cu Kα radiation at a scan rate of 2° min^{-1}, from 2θ = 20° to 80°. The software of the instrument was used for phase identification from the diffractograms.

The adherence test of the catalyst layer onto the substrates was carried out by measuring the weight loss of coating during ultrasonic bath (Testlab TB04, 40 kHz and 160 W) in deionized water at room temperature. Every 30 min of ultrasonic bath the structured catalysts were dried at 130 °C for 60 min and weighted. Six ultrasonic steps of 30 min were performed for each structured catalyst. The percentage of coating retained was analyzed.

2.6. Photocatalytic degradation of NP_4EO by structured catalyst

Two detailed studies were performed using the structured catalyst in heterogeneous photocatalysis reaction aiming to the oxidative degradation of the endocrine-disruptor NP_4EO. In a first step, the catalytic activity and coating stability were evaluated in a synthetic solution containing 10 mg L^{-1} of NP_4EO prepared in distilled and deionized water. In a second step, the role of the water matrix in the performance of the structured catalyst was evaluated. For this proposal, a real

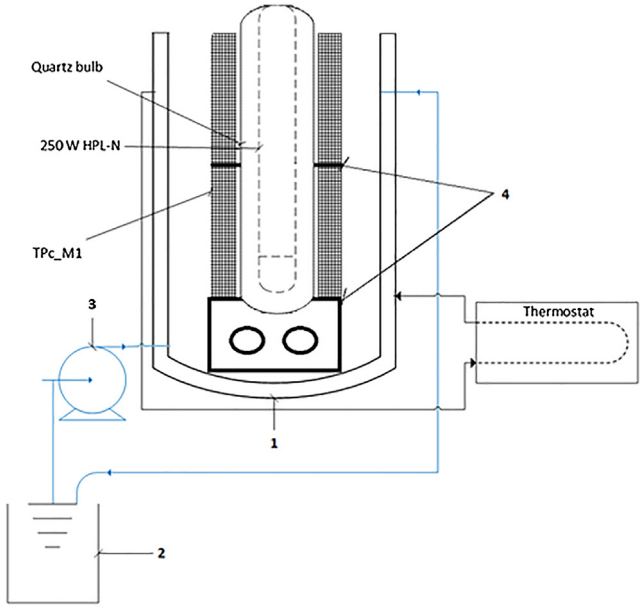

Fig. 1. Scheme of the photocatalytic reactor used in the experiments, where 1 is the borosilicate reactor, **2** is the reservoir, **3** is the peristaltic pump and **4** is the Teflon support.

wastewater was collected after a secondary treatment by activated sludge in the municipal wastewater treatment plant (WWTP) from Novo Hamburgo/Brazil. Before the treatment, a known NP_4EO concentration of 10 mg L^{-1} was added to the real wastewater to ensure that it contains the target pollutant (supplementary material, Fig. S2).

All reactions were carried out by recirculating the solution in a batch reactor operated in recirculation mode. Two structured catalysts were irradiated by a high-pressure mercury vapor lamp (HPL-N, 250 W) without the external glass bulb, placed inside a quartz tube (Fig. 1). These experimental set up is based on previous results [26].

The real wastewater and the samples obtained before and after the photocatalytic reactions were characterized by the following methods: NP_4EO and TOC concentration.

The concentration of NP_4EO was determined by measuring the absorbance of the solution at 272 nm, corresponding to the maximum absorption wavelength of NP_4EO in UV–visible region [27], by a T80 + UV–vis spectrometer (PG Instruments Ltd).

The conversion of NP_4EO from aqueous solutions was calculated by equation (1).

$$X(C) = \frac{Abs_0 - Abs}{Abs_0} \quad (1)$$

where $X\ (C)$ is conversion of NP_4EO, Abs_0 is the initial absorbance of NP_4EO at $\lambda = 270$ nm and Abs is the absorbance of NP_4EO ($\lambda = 270$ nm) at any time.

The kinetics of heterogeneous reaction for the degradation of

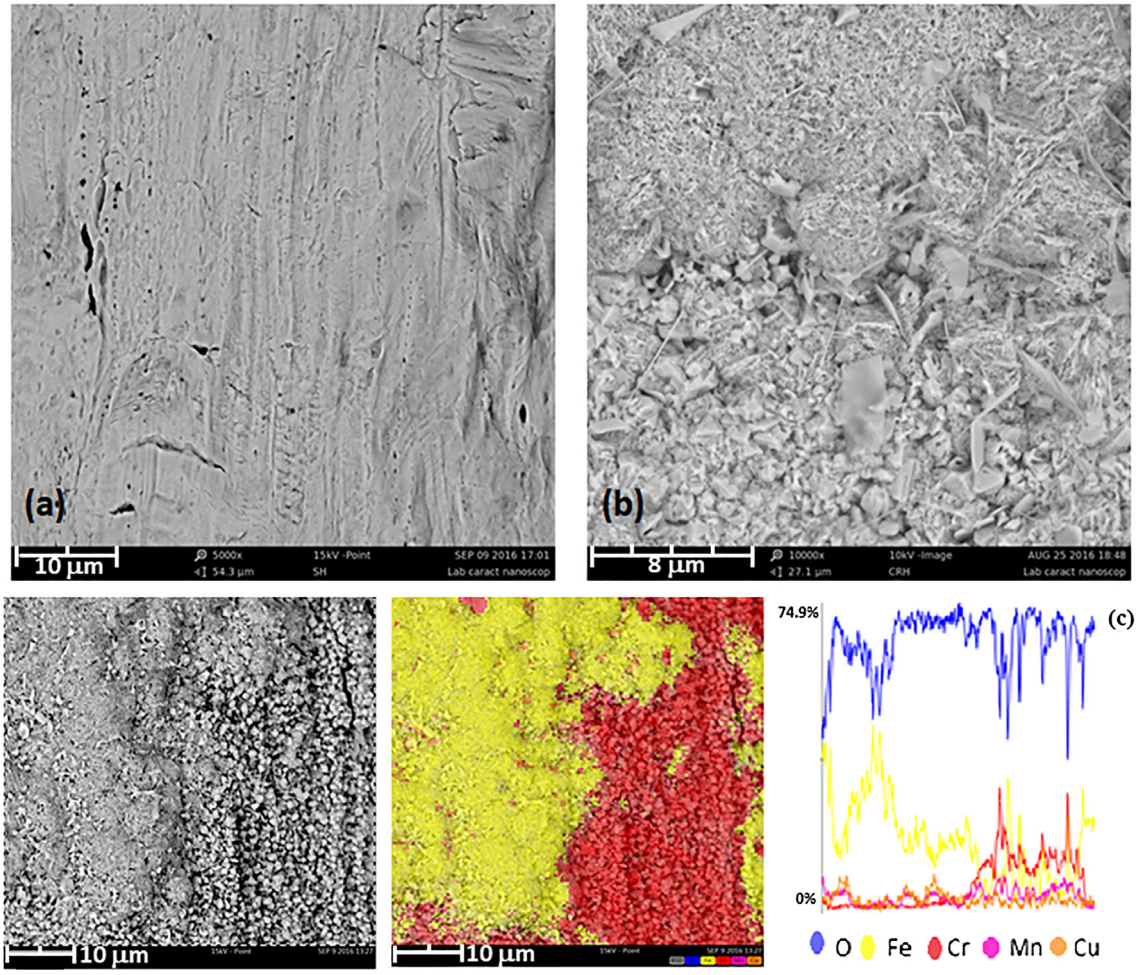

Fig. 2. SEM image of wire mesh before (a) and after (b) thermal pretreatment (900 °C for 120 min at 10 °C min^{-1}). (c) elemental mapping showing the internal surface, constituted by chromium (red) and the outer surface formed by iron (yellow). (For interpretation of the references to colour in this figure legend, the reader is referred to the web version of this article.)

organics can encompasses with both reaction and adsorption that occurs simultaneously [28] and can be described by the Langmuir–Hinshelwood mechanism [29].

$$\frac{C}{C_0} = -e^{k \times t} \tag{2}$$

where C is the NP_4EO concentration at any time ($mg\,L^{-1}$), C_0 is the initial NP_4EO concentration ($mg\,L^{-1}$), t is the treatment time (min) and k is the pseudo first-order rate constant (min^{-1}) for the degradation of NP_4EO.

The total organic carbon (TOC) analysis was carried out using the non-purgeable organic carbon method in a Shimadzu TOC-L CPH analyzer equipped with an automatic sample injector. Based on TOC results, the conversion was calculated following Eq. (3).

$$X(TOC) = \frac{TOC_0 - TOC}{TOC_0} \tag{3}$$

where TOC_0 is the initial TOC and TOC is the TOC at any time.

Besides, NP_4EO and TOC analysis for the real wastewater an ion chromatography (IC) analysis was performed by using a Dionex ICS-3000 DC coupled to a conductivity detector. For anions and cations, the column used were an IonPac® AS23 2 × 250 mm and an IonPac® CS12A 2 × 250 mm, respectively. The eluent consists of 4.5 mM of Na_2CO_3 and 0.8 mM of $NaHCO_3$ for the anions detection and 11 mM of H_2SO_4 for the cations analyzes. The pH was determined by the potentiometric method using a DM-22 Digimed pH-meter.

3. Results and discussion

3.1. Metallic meshes after pretreatment: morphology and species at the surface

SEM micrograph shows the morphology of the metallic mesh before the calcination step (Fig. 2.a). After the calcination, two different morphologies were observed in the surface of the metallic meshes, one with regular grains with sizes about 0.5 μm and another with a smooth aspect, localized in the edge of the wire (Fig. 2.b). On the other hand, the elemental mapping indicated that the internal surface with grain-type morphology is constituted mainly by chromium, while the outer surface is mainly constituted by iron (Fig. 2.c).

The formation of this outer layer at this calcination temperature has not been observed yet. This formation can be attributed to the high heating rate of 10 °C min^{-1}, which promotes the transport of iron (Fe) to the outer surface of the steel, forming oxides and spinels. In fact, this behavior has been reported in the literature, but for higher calcination temperatures and longer times [30]. A scheme for the formation of the oxide layer on the metallic mesh is presented on the supplementary material (Fig. S2).

Fig. 3 shows the Raman spectrum of the calcined metal mesh with the characteristic vibrational bands of different metal oxides, which allows the identification of the oxides formed during the thermal treatment. The characteristic signals of Fe_2O_3 particles are clearly observed at 225, 247, 300, 412, 500, 610, 1100 and 1370 cm^{-1} [31]. Besides, bands at 516 and 660 cm^{-1} are evident, which are associated to the main band of Cr_2O_3 [30] and to the spinel species based on iron, manganese and chromium (Fe_3O_4, $Fe_2Cr_2O_4$ and/or $Mn_{1+x}Cr_{1-x}O_{4-x}$) [32].

3.2. Metallic meshes after washcoating: characterization of the TiO_2 films

Fig. 4 shows the optical images of the metallic meshes M1 and M2 coated with the three suspensions evaluated (TPa, TPb and TPc). An important catalyst particle accumulation at the wire-crossing points was observed, for M2 coatings. These agglomerations produced a non-uniform TiO_2 layer thickness. This type of accumulation is expected when the catalytic coating is produced via washcoating method.

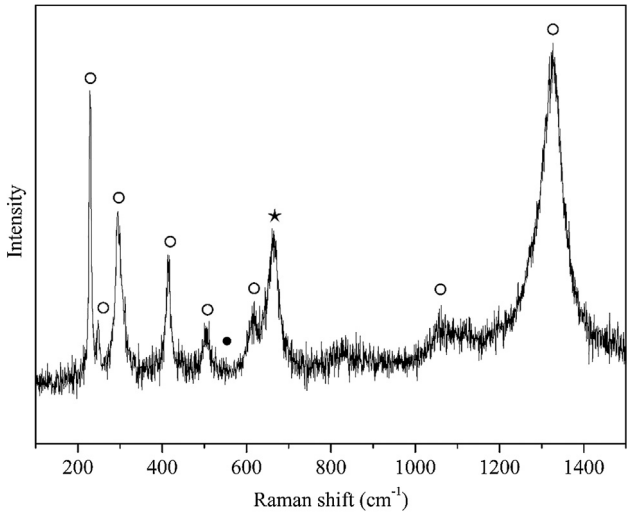

Fig. 3. Raman spectra of wire mesh after thermal pretreatment: (°) Fe_2O_3, (•) Cr_2O_3 and (*) spinel based on iron, manganese and chromium spinels ($Fe_2Cr_2O_4$ and/or $Mn_{1+x}Cr_{1-x}O_{4-x}$).

The coating uniformity was different depending upon the PVA/TiO_2 ratio of the suspension used and on the wire mesh openings. To understand the influence of this non-uniformity in some coatings, adherence tests were accomplished, and the adherence values are presented in Table 1.

Two opposite behaviors were revealed with the adherence tests results. For the higher PVA/TiO_2 ratio, the best adherence results were achieved for the M1 wire-mesh, while the worst were obtained for the M2 wire-mesh. Accumulations at wire intersections for the M2 (mesh opening: 1514 μm) occurred when PVA/TiO_2 ratio increased, resulting in a decrease of the coating adherence to the substrate. For the M1, mesh opening: 546 μm, the behavior was opposite, since, no agglomerations were observed at the crossing of the wires for M1.

These differences can be explained by connecting the substrate structure with the suspension properties. The presence of PVA in the suspension modifies its surface tension and its viscosity, being the suspension a non-Newtonian fluid [15,33]. The suspension viscosity is increased with the PVA addition. The higher viscosity has an important role in two steps of the catalytic coating synthesis: (i) the removal of wire-mesh piece from the suspension and (ii) the elimination of the excess of suspension via air blowing. In both steps, the suspension hydrodynamic depends upon the substrate opening diameter, among others [34].

It is expected that the suspension withdrawal rate increases as the mesh opening increases. M2 presents larger mesh opening than that of M1. Therefore, M2 promotes rapid suspension removal without the time required for the generation of a uniform film layer, turning up in accumulation points, especially in the wire crossing section (Fig. 4, M2). For M1 this removal occurs slowly, producing a uniform coating onto the wire-mesh surface (Fig. 4, M1). Moreover, the rapid withdrawal presented by M2 seems to be one of the reasons for the low adherence values found for all suspensions evaluated.

Fig. 5 shows images of optical microscopy of the systems TPa_M2 and TPc_M2 to compare the differences of morphologies presented by these systems, with better and worst results of adherence to M2 substrate, respectively. Cracks along the coating in TPa_M2 and TPc_M2 were detected. However, in the TPc_M2 sample, deeper cracks located in the wire-crossing were observed. Theses cracks can be responsible for the poor adherence of the coating to the structured substrate [35–37].

The deep cracks in coatings, especially in wire-crossing areas, where the suspension accumulations/agglomeration took place, were originated during the calcination step of the washcoating procedure. A higher concentration of the suspension means a higher amount of

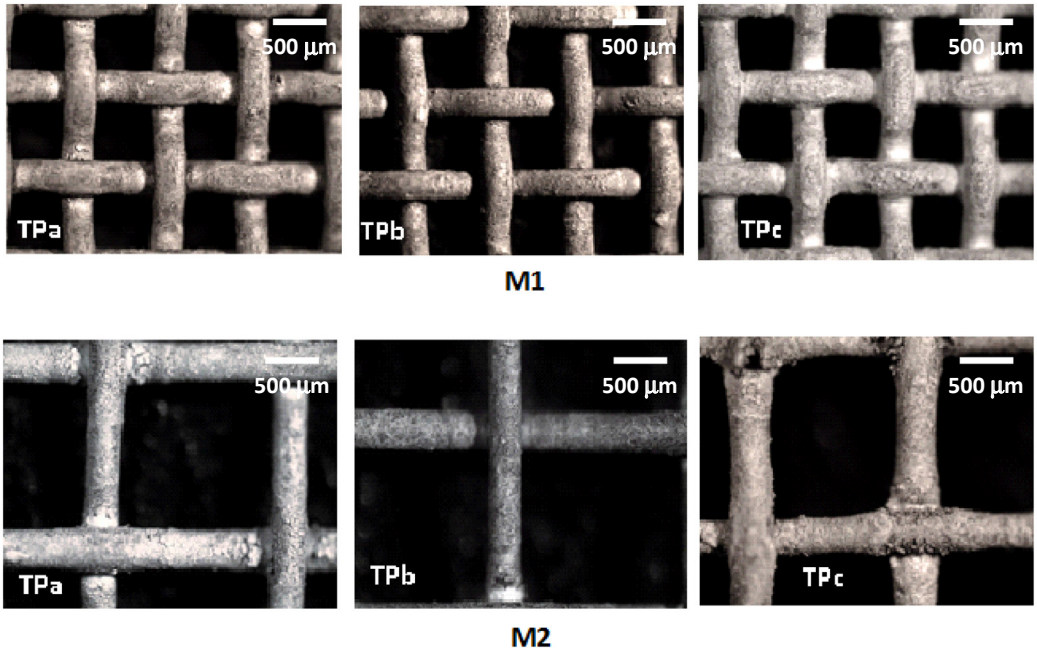

Fig. 4. Optical microscopy images of M1 and M2 metallic-mesh coated with the three suspensions: TPa, TPb and TPc.

Table 1
Adherence percentage of TiO_2 coatings supported in AISI 304 metallic-meshes.

Suspension (PVA/TiO_2 ratio)	Adherence of TiO_2 coatings (%)	
	M1	M2
TPa (0.19)	18	42
TPb (0.28)	74	32
TPc (0.37)	91	20

photographs show that the diameter of coated wires is almost constant along the total longitude, which is an indicative of a uniform distribution of the coating along the substrate surface. This was also confirmed by observing cross section of SEM images of systems TPc_M1 and TPc_M2. In contrast to TPc_M2, the coating obtained from the TPc_M1 system did not show the deep cracks or accumulations of the TPc suspension at the wire-crossing, generating a uniform coating with smooth appearance and high adhesion. The comparison between the

Fig. 5. Images of optical microscopy of the systems (a) TPa_M2 and (b) TPc_M2.

organic additives (PVA). Thus, during the calcination step a stronger release of carbon dioxide from the interior of the catalyst suspension was produced [38].

Based on the data presented in Table 1 and Fig. 5, it is possible to say that the adherence of the coating to the metallic substrate is related to three variables: the structure of the stainless steel metallic-mesh, the thermal pre-treatment and the amount of organic additive (PVA/TiO_2 ratio) used in the suspensions.

The thickness uniformity of the catalytic layer can be estimated by a careful analysis of the images obtained by optical microscopy. In this case, the thickness can be estimated reasonably by measuring the diameter wire before (Fig. 5.c) and after the coating procedure (Fig. 5.a and b), at different locations along the wires of the meshes. These images of the systems aided in the interpretation of the adherence values found for these systems: 91% to TPc_M1 and 20% to TPc_M2.

Surface cracks are observed in both systems in Fig. 6. These cracks were originated during the calcination step by the dewatering of the coating and are characteristic of catalytic coatings obtained from TiO_2 [39], being beneficial to promote the photocatalytic activity to some extent [22,38]. The difference between the expansion coefficients of the metallic substrate and of the catalytic coating can be one of the reasons for the formation of cracks [18]. These superficial cracks did not affect the adherence of the coating to the structured metallic substrate. The TPc_M1 system showed adherence values higher than 90%, even after 180 min under highly intense ultrasound treatment.

Fig. 7 shows the Raman spectrum of the TPc_M1 system. An

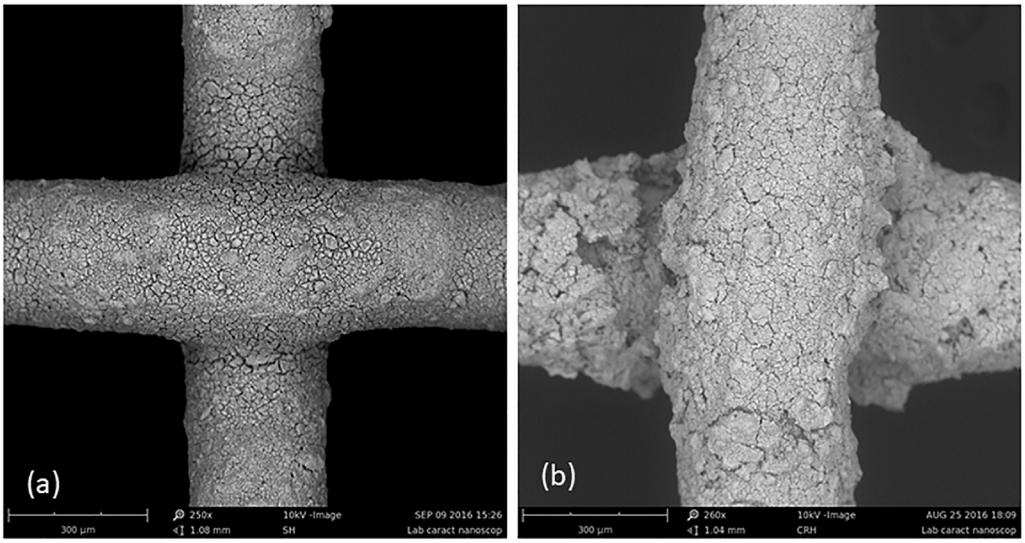

Fig. 6. SEM images of systems (a) TPc_M1 and (b) TPc_M2.

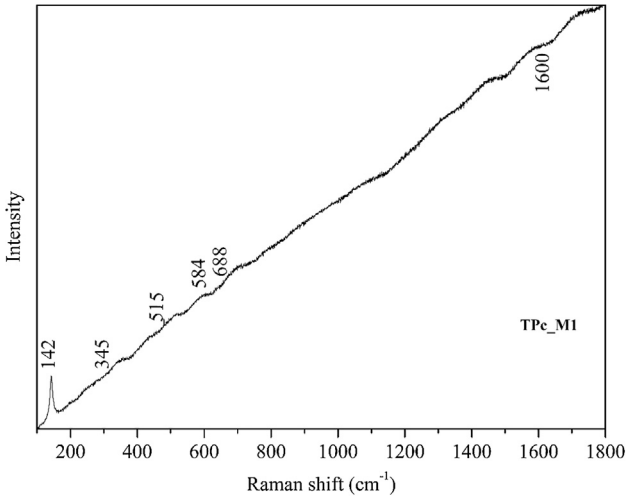

Fig. 7. Raman spectra of TPc_M1.

important fluorescence effect is observed and makes difficult analyzing the spectrum. Nevertheless, the main characteristic band of TiO_2 with anatase structure is identified at 142 cm^{-1}, the other 5 bands at 195, 380, 517 and 660 cm^{-1} are quite small [14]. Besides, the two small bands at 1350 and 1580 cm^{-1} correspond to the C═C bound of the molecular chains of PVA [38]. The presence of this band indicates that not all carbon of the organic additive was converted to CO_2 during the calcination step.

Raman vibration modes of zirconium oxide were not observed. However, the fluorescence effect in the Raman spectrum could be attributed to the ZrO_2 nanoparticles present in the TPc suspension. This fluorescence effect has already been reported in coatings containing nanoparticles in their composition [14].

The identification of the two crystalline phases of TiO_2 is of great importance, because it indicates that the obtained coating can be adequate for photocatalytic purposes. The presence of rutile crystalline phase can be confirmed through the XRD technique. X-ray diffractograms of the TPc_M1 system and that of the calcined powder of the suspension TPc are shown in Fig. 8. The peak of ZrO_2 in the tetragonal

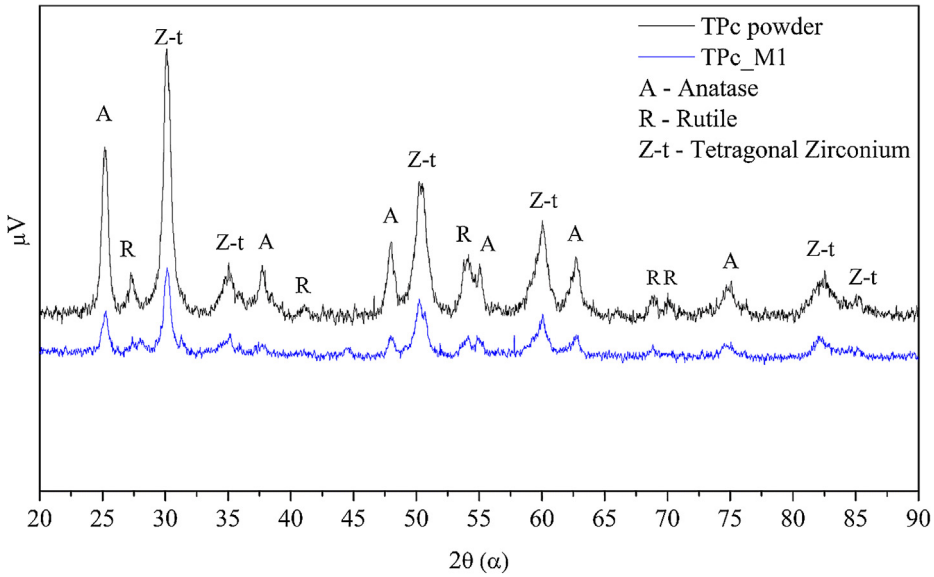

Fig. 8. XRD comparison of TPc_M1 system (black) and calcined powder of the suspension TPc (blue). (For interpretation of the references to colour in this figure legend, the reader is referred to the web version of this article.)

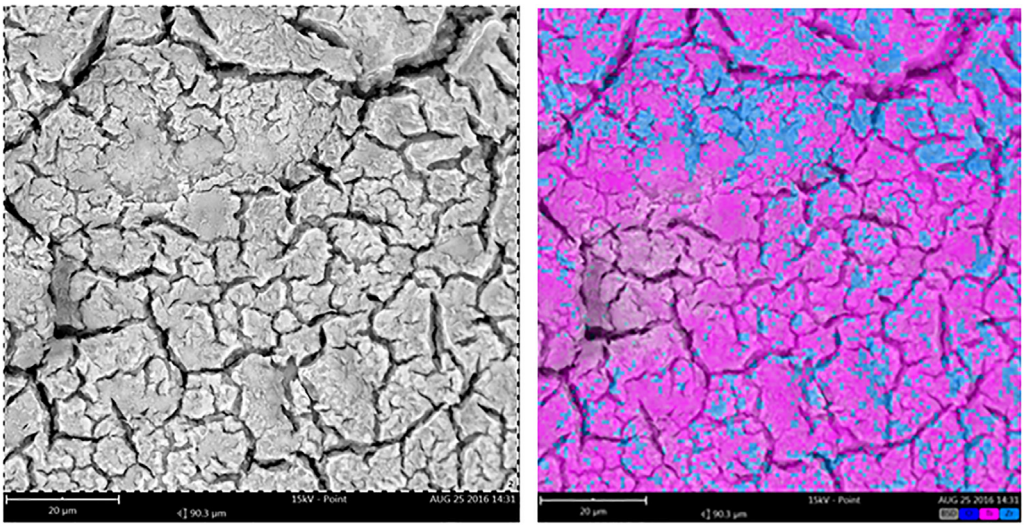

Fig. 9. SEM image of the coating with elemental analysis of the system TPc_M1. Zr (light blue) and Ti (magenta). (For interpretation of the references to colour in this figure legend, the reader is referred to the web version of this article.)

form [40], and the TiO_2 peaks in the rutile and anatase phases [10,20] were observed, thus confirming the bands observed in the Raman spectrum (Fig. 7).

Fig. 9 shows a SEM image with the elemental analysis of the system TPc_M1. The presence TiO_2 and ZrO_2 incorporated into the coating and uniformly distributed at the surface of the structured metallic substrate is shown.

The identification of both crystalline phases, anatase and rutile, is an indication that the amount of ZrO_2 nanoparticles present in the suspension did not interfere in the stability of these phases. Literature reports that the use of a high molar ratio Zr/TiO_2 leads to a stabilization/formation of anatase in a higher proportion than rutile [18,21]. Another variable that should be considered in obtaining a coating of TiO_2 with the two photocatalytic active phases is the polarity of the solvent, since a protic solvent forms easily and preferably the anatase crystalline phase of the TiO_2 [41]. Temperature of the calcination step contributes for obtaining/stabilizing the anatase and rutile phases. By using high temperatures, the catalytic coating presents only the anatase phase [13].

Considering the above-mentioned variables: temperature and polarity of the TPc suspension, are in the correct direction for obtaining an adequate catalytic coating, probably with good photocatalytic activity.

Bands of the metallic substrate were not observed by Raman (Fig. 7) or by elemental mapping techniques (Fig. 9), thus confirming a uniform morphology and thickness and also high homogeneity of the TPc coating onto the M1 substrate.

3.3. Evaluation of the structured catalysts in the photocatalytic degradation of NP_4EO

The best structured catalyst TPc_M1 (PVA/TiO_2 mass ratio of 0.37, mesh opening of 546 μm and 2 wt% of TiO_2 loading) was applied in heterogeneous photocatalytic reaction aiming the oxidative degradation of the NP_4EO.

Fig. 10 presents the spectral changes of NP_4EO during the photocatalytic treatment of the synthetic solution at different treatment times. There are two absorbance peaks at 199 and 225 nm and another one at 277 nm. The peak at 199 nm is ascribed to the C=C from the aromatic form, whereas 225 nm corresponds to the CΞC in the ethos group. The other peak at 277 nm is assigned to the C = O from benzene ring [7,42].

All peaks almost disappeared at 60 min of reaction due to the destruction of C=C, CΞC and C=O bonds in the chromophore structure of

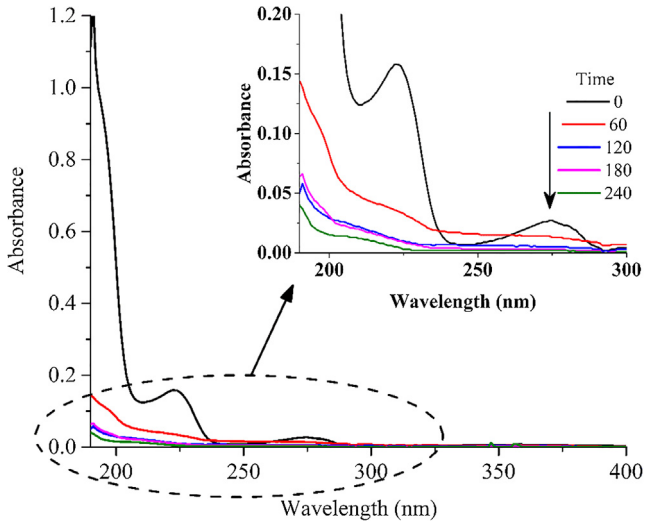

Fig. 10. UV–vis spectra during the photocatalytic treatment of the synthetic solution containing NP_4EO by TPc_M1. Experimental conditions: NP_4EO = 10 mg L^{-1}; pH = 5 and room temperature.

NP_4EO. It means that all NP_4EO is attacked by the hydroxyl radical ($HO^{\cdot}$) generated at the catalyst surface and/or by absorbing UV photons. Furthermore, the absorbance peaks did not increase, meaning that no intermediates that absorbs in UV–vis spectra were generated during the photocatalytic degradation. Similar spectra for heterogeneous photocatalysis using a commercial Ti-TiO_2® mesh at treatment time of 0 and 240 min were found in a previous work [9].

Fig. 11.a depicts the profile of NP_4EO degradation with time exhibiting a NP_4EO conversion of 91% (Eq. (1) at the treatment time of 240 min. A work carried out by Solcova et al. [43] with a TiO_2 thin layer and that employed initial NP_4EO concentration of 10 mg L^{-1} (final volume of 200 mL) reports that a NP_4EO removal of 91% was achieved in the same treatment time of 240 min. Another literature report performed by Dzimin et al. [44] informed 85% of contaminant removal using a TiO_2-membrane. The result obtained by our group was similar or even better to that found in some representative works, with the advantage of using a final higher volume of 5 L.

Fig. 11.a also shows that the NP_4EO degradation with time follows an exponential trend, which may describe the degradation of NP_4EO according to the first-order kinetic reaction (Eq. (2).

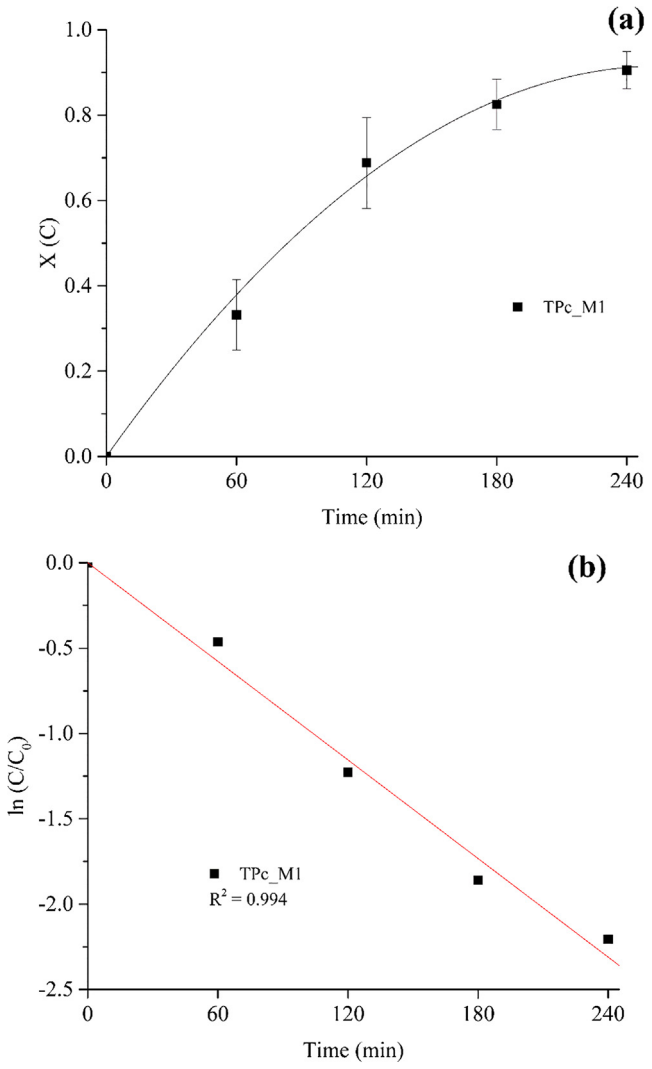

Fig. 11. (a) Degradation profile of NP_4EO on the treatment of synthetic solution by heterogeneous photocatalysis with TPc_M1. (b) Langmuir–Hinshelwood model plot of reaction rate.

The slope of the straight line for a plot of $\ln(C/C_0)$ versus time (min) in Fig. 11.b determines the k value resulting in 0.0096 min^{-1}. This work, using an initial concentration of NP_4EO of 10 mg L^{-1}, achieved 91% of removal and can be compared with a previous work [9], using 50 mg L^{-1}, where 87% of degradation and 0.0084 min^{-1} reaction kinetics were obtained. On the other hand, this finding does not appear to be related to mineralization. The results of UV–vis spectroscopy, usually used to evaluate the degradation of NP_4EO, do not show organic byproducts molecules that could be formed, disturbing the evaluation of the final photocatalytic conversion.

Comparing the results at 240 min, between this work and the previous one [9], with an initial concentration of NP_4EO of 10 mg L^{-1} and 50 mg L^{-1}, mineralization was found to be 21% and 63% (Eq. (3), respectively.

As previously reported [9], an important step on the NP_4EO degradation was the reduction of the absorption band in the UV spectrum by the UV radiation emitted by the 250 W HPL-N lamp (direct photolysis). However, this step does not lead to the NP_4EO mineralization. On the other hand, the TOC abatement is related to the hydroxyl radical generated on the catalyst surface. Furthermore, the Langmuir–Hinshelwood model (equation (2) postulates that the reaction of the species adsorbed on the surface is the rate-limiting step. In this case, the species present in the reaction should adsorb on a fixed number of active sites

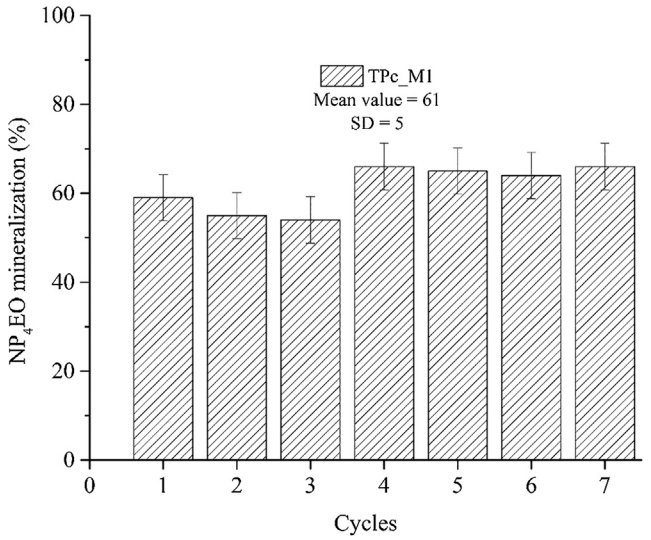

Fig. 12. NP_4EO mineralization (synthetic solution) in the long-term stability test using TPc_M1 in the heterogeneous photocatalytic reaction.

[45] to react with $HO^{\cdot}$, leading to mineralization. In this context, a higher amount of NP_4EO contaminant will be mineralized in a more efficient way with the $HO^{\cdot}$ generated than a lower NP_4EO concentration.

In order to analyze the durability of the TPc_M1 composite, 7 cycles of 600 min each one was performed, and the mineralization was inferred by the decrease of the total organic carbon.

Fig. 12 shows that the TPc_M1 composite catalyst exhibited excellent stability, without losing activity for the mineralization of NP_4EO. Conversely the stability of TPc_M1 were higher than the ones obtained by TiO_2-foam used on a previous work [14]. The TiO_2-foam was applied in the mineralization of NP_4EO and presented a decline in the NP_4EO mineralization associated to a poisoning of the catalyst after seven reuse cycles [14]. The previously catalytic deactivation (TiO_2-foam) was attributed to adsorption of degradation byproducts on the active sites, hindering the formation of hydroxyl radicals. The best stability of TPc_M1 composite catalyst is mainly attributed to three reasons: (i) the substrate structure that improves the flow through the TPc_M1 composite, (ii) the composition of PVA/TiO_2 ratio and (iii) the polarity of the TPc suspension in the washcoating method.

The introduced changes in PVA/TiO_2 ratio in the washcoating procedure induced the obtaining of a stable and well dispersed catalytic coating, without deep cracks or accumulations of the TPc suspension at the wire-crossing. In fact, the PVA is being removed from the surface of the catalyst with the use, releasing more active sites [24,46]. Therefore, an increase in the mineralization of NP_4EO was observed. In consequence, the deposit of byproducts on the TPc_M1 surface was avoided.

It is known that pH has a significant impact in heterogeneous photocatalysis reaction, which directly affects the oxidative degradation of contaminants by $HO^{\cdot}$ [47]. Different reports analyze the influence of the initial pH on the degradation of NP_nEO, showing that pH = 5 or less presented the best results [48]. These findings can be explained considering that the adsorption of organics depends on the nature of the catalyst and of the solutions [48]. For TiO_2, the zero charge point (PZC) is around 6 [49]. Under acidic conditions, the PZC potential of TiO_2 is positive and NP_4EO is in anionic form, which represents an advantage to the adsorption of NP_4EO, promoting the NP_4EO degradation. In the present work, the initial pH of the solution was 5 ± 0.3 and, after the treatment time, no significant differences in pH values were observed.

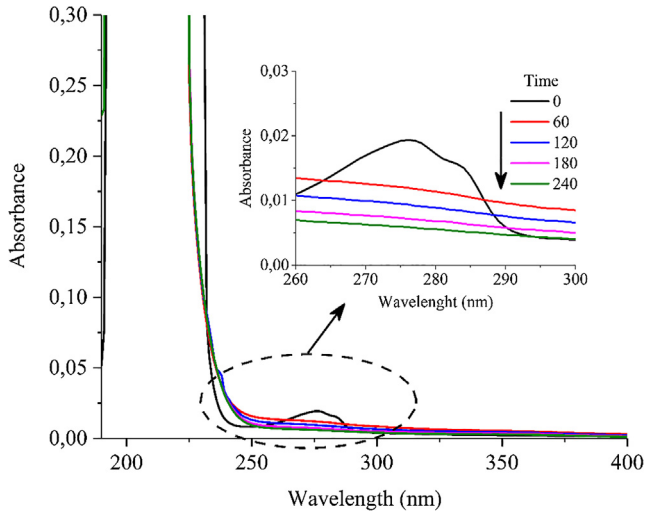

Fig. 13. Changes in UV–vis spectra during the photocatalytic degradation of wastewater containing NP_4EO by TPc_M1.

3.4. The role of water matrix in the performance of the TPc_M1 catalyst

Fig. 13 shows the spectral changes of the wastewater containing the NP_4EO before and after the treatment by photocatalysis on TPc_M1. The NP_4EO degradation is like the one previously presented in Fig. 10 for synthetic solutions, i.e., the characteristic peak of NP_4EO also disappeared after 60 min in the real wastewater matrix due to the destruction of the chromophore structure.

The degradation of the NP_4EO, related to the time of reaction, was calculated based on equation (1). Fig. 14a shows these results for the NP_4EO in the real wastewater. Comparing with the results obtained with the synthetic solution ($X\ (C) = 91\%$ and $k = 0.0096\ min^{-1}$, Fig. 10), it is observed a reduction in the degradation of NP_4EO (57%) and, therefore, there is also a decrease in the degradation rate ($k = 0.00369\ min^{-1}$).

The real wastewater has a content of organic matter presented as an initial TOC of $7\ mg\ L^{-1}$, before the addition of NP_4EO. This organic matter can have an influence on the photocatalytic treatment. The reduction in the NP_4EO degradation rate can be therefore most attributed to the UV radiation scavenger, the organic matter, present in the real wastewater matrix [9]. Other important factor is that NP_4EO have an exceptional ability to form colloids by the agglomeration with organic matter [50]. Consequently, there is a competition by the active sites on the TPc_M1 catalyst, leading to a decrease in the degradation rate.

Fig. 14.a also shows the mineralization profile of the organic compounds present on the wastewater matrix containing NP_4EO. By equation (3), a mineralization of 17% was found on TPc_M1. This mineralization (17%) is smaller than the one previously obtained (21%) with the synthetic solution. In fact, the organic compounds present in the real wastewater matrix can interact with the UV radiation and a photolysis process can consume UV, decreasing the UV radiation arriving at the catalyst surface. As a consequence, less hydroxyl radicals are available for the mineralization reaction [51]. On the other side, the initial TOC content is higher for the wastewater containing NP_4EO ($12\ mg\ L^{-1}$) than for the synthetic solution ($8\ mg\ L^{-1}$). It is then expected that more time will be necessary to achieve the same mineralization.

Furthermore, the catalytic activity of TPc_M1 to $HO^{\cdot}$ generation can be associated to the initial chemical composition of the real wastewater (supplementary material, Table S2). According to Halmann et al. [52], the nitrite ion can be converted in nitrate by two $HO^{\cdot}$ scavenger according to the proposed mechanisms (Eq. (4)).

$$2\ HO^{\cdot} + NO_2^{-} \rightarrow NO_3^{-} + H_2O \quad (4)$$

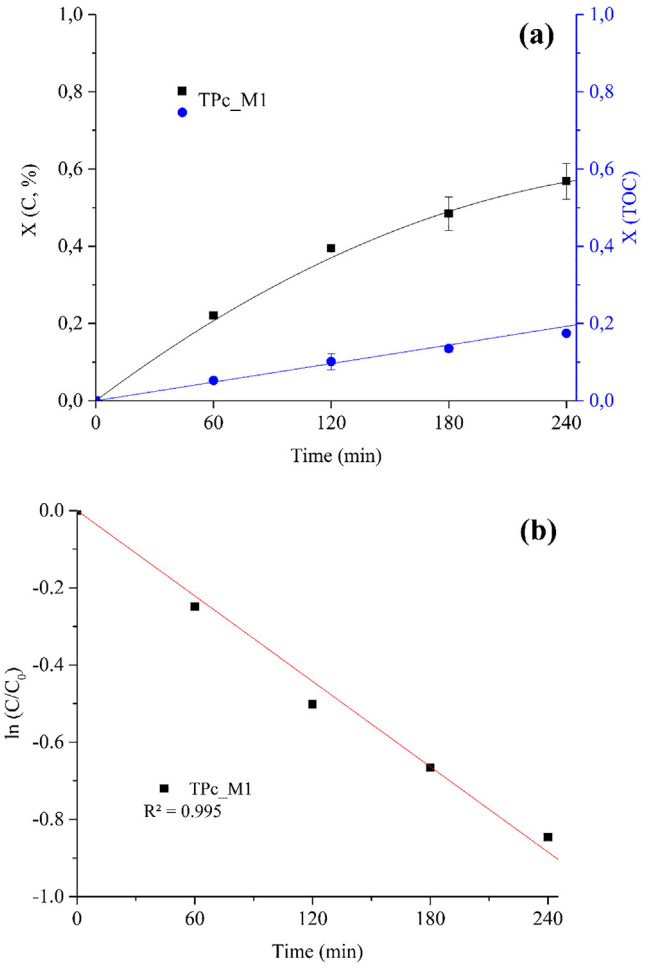

Fig. 14. (a) Degradation of NP_4EO and mineralization profile of organic matter present in real wastewater on TPc_M1 samples in heterogeneous photocatalysis reaction. (b) Langmuir–Hinshelwood model plot of reaction rate.

Halmann et al. [52] explain that the proposed mechanism of equation (4) involves the surface of structured catalysts adsorbing nitrite ions, with consequent interaction with $HO^{\cdot}$ according to the Langmuir-Hinshelwood mechanism. In fact, by the treatment with real wastewater the nitrite concentration decreases from $155\ mg\ L^{-1}$ to $14\ mg\ L^{-1}$. On the other hand, the nitrate concentration increases from $192\ mg\ L^{-1}$ to $335\ mg\ L^{-1}$. This fact leads to competition with organic contaminants adsorbed, with changes in the rate of mineralization at real wastewater containing NP_4EO [51].

4. Conclusions

This work brings new insights about the synthesis procedure of TiO_2 coatings with high adherence onto stainless steel meshes, keeping unaltered its main features and the anatase/rutile proportion.

The TPc_M1 structured system was an active and highly stable photocatalyst. In addition, the TiO_2 coating kept, after being used several times under reaction conditions, similar catalytic activity from the initial tests. The better results were related to the wire opening of the metal mesh, thermal pre-treatment and PVA/TiO_2 ratio used in the washcoating.

In the synthetic solution, that system provided NP_4EO degradation of 91% and mineralization of 60%. In fact, these results do not change significantly when the structured catalyst was applied to a real wastewater matrix spiked with target NP_4EO contaminant.

Acknowledgements

The authors would like to acknowledge the financial support of CNPq, FAPERGS, FINEP, CAPES and CAPG-BA 73/14 490 from Brazil and of ANPCyT, CONICET, CAPG-BA 73/14, and UNL from Argentina.

References

[1] K.H. Langford, J.N. Lester, Fate and behavior of endocrine disrupters in sludge treatment and disposal, in: J. Birkett, J. Lester (Eds.), Endocrine Disrupters Wastewater and Sludge Treatment Processes, 1st ed., Taylor & Francis Group, Boca Raton, 2002, pp. 4–42 https://www.taylorfrancis.com/books/9781420032185.

[2] R. Renner, European bans on surfactant trigger transatlantic debate, Environ. Sci. Technol. 31 (1997) 316A–320A, http://dx.doi.org/10.1021/es972366q.

[3] R. Goto, T. Kubota, Y. Ibuki, K. Kaji, A. Goto, Degradation of nonylphenol polyethoxylates by ultraviolet B irradiation and effects of their products on mammalian cultured cells, Toxicology 202 (2004) 237–247, http://dx.doi.org/10.1016/j.tox.2004.05.017.

[4] M. Abbas, M. Adil, S. Ehtisham-ul-Haque, B. Munir, M. Yameen, A. Ghaffar, G.A. Shar, M. Asif Tahir, M. Iqbal, Vibrio fischeri bioluminescence inhibition assay for ecotoxicity assessment: a review, Sci. Total Environ. 626 (2018) 1295–1309, http://dx.doi.org/10.1016/j.scitotenv.2018.01.066.

[5] M. Iqbal, Vicia faba bioassay for environmental toxicity monitoring: A review, Chemosphere 144 (2016) 785–802, http://dx.doi.org/10.1016/j.chemosphere.2015.09.048.

[6] M. Neamţu, F.H. Frimmel, Photodegradation of endocrine disrupting chemical nonylphenol by simulated solar UV-irradiation, Sci. Total Environ. 369 (2006) 295–306, http://dx.doi.org/10.1016/j.scitotenv.2006.05.002.

[7] L. Chen, H. yun Zhou, Q. ying Deng, Photolysis of nonylphenol ethoxylates: The determination of the degradation kinetics and the intermediate products, Chemosphere 68 (2007) 354–359, http://dx.doi.org/10.1016/j.chemosphere.2006.12.055.

[8] M. Iqbal, I.A. Bhatti, Gamma radiation/H_2O_2 treatment of a nonylphenol ethoxylates: Degradation, cytotoxicity, and mutagenicity evaluation, J. Hazard. Mater. 299 (2015) 351–360, http://dx.doi.org/10.1016/j.jhazmat.2015.06.045.

[9] S.W. da Silva, C.R. Klauck, M.A. Siqueira, A.M. Bernardes, Degradation of the commercial surfactant nonylphenol ethoxylate by advanced oxidation processes, J. Hazard. Mater. 282 (2015) 241–248, http://dx.doi.org/10.1016/j.jhazmat.2014.08.014.

[10] A. Ashar, M. Iqbal, I.A. Bhatti, M.Z. Ahmad, K. Qureshi, J. Nisar, I.H. Bukhari, Synthesis, characterization and photocatalytic activity of ZnO flower and pseudosphere: nonylphenol ethoxylate degradation under UV and solar irradiation, J. Alloys Compd. 678 (2016) 126–136, http://dx.doi.org/10.1016/j.jallcom.2016.03.251.

[11] Y. Wang, M. Zhong, F. Chen, J. Yang, Visible light photocatalytic activity of TiO_2/D-PVA for MO degradation, Appl. Catal. B Environ. 90 (2009) 249–254, http://dx.doi.org/10.1016/j.apcatb.2009.03.032.

[12] S.G. Kumar, K.S.R.K. Rao, Comparison of modification strategies towards enhanced charge carrier separation and photocatalytic degradation activity of metal oxide semiconductors (TiO_2, WO_3 and ZnO), Appl. Surf. Sci. 391 (2017) 124–148, http://dx.doi.org/10.1016/j.apsusc.2016.07.081.

[13] Y. Chen, D.D. Dionysiou, Correlation of structural properties and film thickness to photocatalytic activity of thick TiO_2 films coated on stainless steel, Appl. Catal. B Environ. 69 (2006) 24–33, http://dx.doi.org/10.1016/j.apcatb.2006.05.002.

[14] S.W. da Silva, J.P. Bortolozzi, E.D. Banús, A.M. Bernardes, M.A. Ulla, TiO_2 thick films supported on stainless steel foams and their photoactivity in the nonylphenol ethoxylate mineralization, Chem. Eng. J. 283 (2016) 1264–1272, http://dx.doi.org/10.1016/j.cej.2015.08.057.

[15] E.D. Banús, O. Sanz, V.G. Milt, E.E. Miró, M. Montes, Development of a stacked wire-mesh structure for diesel soot combustion, Chem. Eng. J. 246 (2014) 353–365, http://dx.doi.org/10.1016/j.cej.2014.02.086.

[16] L. del Río, I. López, G. Marbán, Stainless steel wire mesh-supported Co3O4 catalysts in the steam reforming of ethanol, Appl. Catal. B Environ. 150–151 (2014) 370–379, http://dx.doi.org/10.1016/j.apcatb.2013.12.022.

[17] X.B. Gong, S.J. You, X.H. Wang, J.N. Zhang, Y. Gan, N.Q. Ren, A novel stainless steel mesh/cobalt oxide hybrid electrode for efficient catalysis of oxygen reduction in a microbial fuel cell, Biosens. Bioelectron. 55 (2014) 237–241, http://dx.doi.org/10.1016/j.bios.2013.12.015.

[18] K.S. Yang, G. Mul, J.S. Choi, J.A. Moulijn, J.S. Chung, Development of TiO_2/Ti wire-mesh honeycomb for catalytic combustion of ethyl acetate in air, Appl. Catal. A Gen. 313 (2006) 86–93, http://dx.doi.org/10.1016/j.apcata.2006.07.008.

[19] P.J. Lee, C.C. Ho, C.S. Hwang, S.J. Ding, Improved physicochemical properties and biocompatibility of stainless steel implants by PVA/ZrO_2-based composite coatings, Surf. Coat. Technol. 258 (2014) 374–380, http://dx.doi.org/10.1016/j.surfcoat.2014.08.066.

[20] B. Babiarczuk, A. Szczurek, A. Donesz-Sikorska, I. Rutkowska, J. Krzak, The influence of an acid catalyst on the morphology, wettabillity, adhesion and chemical structure properties of TiO_2 and ZrO_2 sol-gel thin films, Surf. Coatings Technol. 285 (2016) 134–145, http://dx.doi.org/10.1016/j.surfcoat.2015.11.030.

[21] T. Cai, Y. Liao, Z. Peng, Y. Long, Z. Wei, Q. Deng, Photocatalytic performance of TiO_2 catalysts modified by H3PW12O40, ZrO_2 and CeO_2, J. Environ. Sci. 21 (2009) 997–1004, http://dx.doi.org/10.1016/S1001-0742(08)62374-8.

[22] M. Ren, F.H. Frimmel, G. Abbt-Braun, Multi-cycle photocatalytic degradation of bezafibrate by a cast polyvinyl alcohol/titanium dioxide (PVA/TiO_2) hybrid film, J. Mol. Catal. A Chem. 400 (2015) 42–48, http://dx.doi.org/10.1016/j.molcata.2015.02.004.

[23] L. Liu, C. Zhao, F. Yang, TiO_2 and polyvinyl alcohol (PVA) coated polyester filter in bioreactor for wastewater treatment, Water Res. 46 (2012) 1969–1978, http://dx.doi.org/10.1016/j.watres.2012.01.017.

[24] P. Hegedűs, E. Szabó-Bárdos, O. Horváth, P. Szabó, K. Horváth, Investigation of a TiO_2 photocatalyst immobilized with poly(vinyl alcohol), Catal. Today. 284 (2017) 179–186, http://dx.doi.org/10.1016/j.cattod.2016.11.050.

[25] D.M. Fernandes, J.L. Andrade, M.K. Lima, M.F. Silva, L.H.C. Andrade, S.M. Lima, A.A.W. Hechenleitner, E.A.G. Pineda, Thermal and photochemical effects on the structure, morphology, thermal and optical properties of PVA/Ni0.04Zn0.96O and PVA/Fe 0.03Zn0.97O nanocomposite films, Polym. Degrad. Stab. 98 (2013) 1862–1868, http://dx.doi.org/10.1016/j.polymdegradstab.2013.05.003.

[26] S.W. da Silva, C. Viegas, J.Z. Ferreira, M.A. Rodrigues, A.M. Bernardes, The effect of the UV photon flux on the photoelectrocatalytic degradation of endocrine-disrupting alkylphenolic chemicals, Environ. Sci. Pollut. Res. 23 (2016) 19237–19245, http://dx.doi.org/10.1007/s11356-016-7121-3.

[27] N. Márquez, B. Bravo, G. Chávez, F. Ysambertt, J.L. Salager, Analysis of polyethoxylated surfactants in microemulsion-oil-water systems, Anal. Chim. Acta. 405 (2000) 267–275, http://dx.doi.org/10.1016/S0003-2670(99)00759-X.

[28] W. Xu, J.S. Kong, Y.-T.E. Yeh, P. Chen, Single-molecule nanocatalysis reveals heterogeneous reaction pathways and catalytic dynamics, Nat. Mater. 7 (2008) 992–996, http://dx.doi.org/10.1038/nmat2319.

[29] K.V. Kumar, K. Porkodi, F. Rocha, Langmuir-Hinshelwood kinetics – a theoretical study, Catal. Commun. 9 (2008) 82–84, http://dx.doi.org/10.1016/j.catcom.2007.05.019.

[30] N. Karimi, F. Riffard, F. Rabaste, S. Perrier, R. Cueff, C. Issartel, H. Buscail, Characterization of the oxides formed at 1000 °C on the AISI 304 stainless steel by X-ray diffraction and infrared spectroscopy, Appl. Surf. Sci. 254 (2008) 2292–2299, http://dx.doi.org/10.1016/j.apsusc.2007.09.018.

[31] M. Oćwieja, A. Węgrzynowicz, J. Maciejewska-Prończuk, P. Michorczyk, Z. Adamczyk, M. Roman, E. Bielańska, Preparation of iron oxide nanoparticles doped by chromium for application in water–gas shift reaction, Colloids Surfaces A Physicochem. Eng. Asp. 523 (2017) 71–80, http://dx.doi.org/10.1016/j.colsurfa.2017.04.004.

[32] J.P. Bortolozzi, E.D. Banús, V.G. Milt, L.B. Gutierrez, M.A. Ulla, The significance of passivation treatments on AISI 314 foam pieces to be used as substrates for catalytic applications, Appl. Surf. Sci. 257 (2010) 495–502, http://dx.doi.org/10.1016/j.apsusc.2010.07.019.

[33] L.C. Almeida, F.J. Echave, O. Sanz, M.A. Centeno, J.A. Odriozola, M. Montes, Washcoating of metallic monoliths and microchannel reactors, Stud. Surf. Sci. Catal. (2010) 25–33, http://dx.doi.org/10.1016/S0167-2991(10)75004-7.

[34] P. Huzyak, K. Koelling, The penetration of a long bubble through a viscoelastic fluid in a tube, J. Nonnewton. Fluid Mech. 71 (1997) 73–88, http://dx.doi.org/10.1016/S0377-0257(97)00002-5.

[35] T.T. Vu, L. del Río, T. Valdés-Solís, G. Marbán, Stainless steel wire mesh-supported ZnO for the catalytic photodegradation of methylene blue under ultraviolet irradiation, J. Hazard. Mater. 246–247 (2013) 126–134, http://dx.doi.org/10.1016/j.jhazmat.2012.12.009.

[36] L. Yang, Z. Li, H. Jiang, W. Jiang, R. Su, S. Luo, Y. Luo, Photoelectrocatalytic oxidation of bisphenol a over mesh of TiO_2/graphene/Cu_2O, Appl. Catal. B Environ. 183 (2016) 75–85, http://dx.doi.org/10.1016/j.apcatb.2015.10.023.

[37] S. Naraginti, F.B. Stephen, A. Radhakrishnan, A. Sivakumar, Zirconium and silver co-doped TiO2 nanoparticles as visible light catalyst for reduction of 4-nitrophenol, degradation of methyl orange and methylene blue, Spectrochim. Acta - Part A Mol. Biomol. Spectrosc. 135 (2015) 814–819, http://dx.doi.org/10.1016/j.saa.2014.07.070.

[38] Y. Song, J. Zhang, H. Yang, S. Xu, L. Jiang, Y. Dan, Preparation and visible light-induced photo-catalytic activity of H-PVA/TiO_2 composite loaded on glass via sol-gel method, Appl. Surf. Sci. 292 (2014) 978–985, http://dx.doi.org/10.1016/j.apsusc.2013.12.090.

[39] M.B. Zakaria, M.A. Elmorsi, E.-Z.M. Ebeid, Nanostructured TiO_2 coated stainless steel for corrosion protection, J. Nanosci. Nanotechnol. 16 (2016), http://dx.doi.org/10.1166/jnn.2016.12893.

[40] E.D. Banús, M.A. Ulla, E.E. Miró, V.G. Milt, Co,Ba,K/ZrO_2 coated onto metallic foam (AISI 314) as a structured catalyst for soot combustion: catalytic activity and stability, Appl. Catal. A Gen. 393 (2011) 9–16, http://dx.doi.org/10.1016/j.apcata.2010.11.018.

[41] B.M. Pirzada, N.A. Mir, N. Qutub, O. Mehraj, S. Sabir, M. Muneer, Synthesis, characterization and optimization of photocatalytic activity of TiO_2/ZrO_2 nanocomposite heterostructures, Mater. Sci. Eng. B Solid-State Mater. Adv. Technol. 193 (2015) 137–145, http://dx.doi.org/10.1016/j.mseb.2014.12.005.

[42] D.A. Skoog, F.J. Holler, S.R. Crouch, Principles of Instrumental analysis, 2007. doi: http://dx.doi.org/10.1017/CBO9781107415324.004.

[43] D. Treatment, C. Republic, L.S. Academy, C. Republic, Y.M. Academy, C. Republic, M.M. Academy, C. Republic, Photocatalytic water treatment on TiO2 thin layers, Desalin. Water Treat. 57 (2015) 11631–11638, http://dx.doi.org/10.1080/19443994.2015.1049964.

[44] H. Dzinun, M.H.D. Othman, A.F. Ismail, M.H. Puteh, M.A. Rahman, J. Jaafar, Photocatalytic degradation of nonylphenol by immobilized TiO_2 in dual layer hollow fibre membranes, Chem. Eng. J. 269 (2015) 255–261, http://dx.doi.org/10.1016/j.cej.2015.01.114.

[45] D. Chen, A.K. Ray, Photodegradation kinetics of 4-nitrophenol in TiO_2 suspension, Water Res. 32 (1998) 3223–3234, http://dx.doi.org/10.1016/S0043-1354(98)00118-3.

[46] M. Abdelaziz, M.M. Ghannam, Influence of titanium chloride addition on the optical and dielectric properties of PVA films, Phys. B Condens. Matter. 405 (2010) 958–964, http://dx.doi.org/10.1016/j.physb.2009.10.030.
[47] N.A. Zubir, C. Yacou, X. Zhang, J.C. Diniz Da Costa, Optimisation of graphene oxide-iron oxide nanocomposite in heterogeneous Fenton-like oxidation of Acid Orange 7, J. Environ. Chem. Eng. 2 (2014) 1881–1888, http://dx.doi.org/10.1016/j.jece.2014.08.001.
[48] Y. Xin, M. Gao, Y. Wang, D. Ma, Photoelectrocatalytic degradation of 4-nonylphenol in water with WO_3/TiO_2 nanotube array photoelectrodes, Chem. Eng. J. 242 (2014) 162–169, http://dx.doi.org/10.1016/j.cej.2013.12.068.
[49] H. Selcuk, M. Bekbolet, Photocatalytic and photoelectrocatalytic humic acid removal and selectivity of TiO_2 coated photoanode, Chemosphere 73 (2008) 854–858, http://dx.doi.org/10.1016/j.chemosphere.2008.05.069.
[50] D. Gao, Z. Li, J. Guan, H. Liang, Seasonal variations in the concentration and removal of nonylphenol ethoxylates from the wastewater of a sewage treatment plant, J. Environ. Sci. (China) 54 (2017) 217–223, http://dx.doi.org/10.1016/j.jes.2016.02.005.
[51] P.M. Nagarnaik, B. Boulanger, Advanced oxidation of alkylphenol ethoxylates in aqueous systems, Chemosphere 85 (2011) 854–860, http://dx.doi.org/10.1016/j.chemosphere.2011.06.105.
[52] M.M. Halmann, Photodegradation of Water Pollutants, CRC Press, 1995 (accessed October 20, 2017).